Available online at www.sciencedirect.com
ScienceDirect
Journal of the European Ceramic Society 29 (2009) 1309–1322
www.elsevier.com/locate/jeurceramsoc

Experimental analysis of the evolution of thermal shock damage using transit time measurement of ultrasonic waves

F. Damhof [a,*], W.A.M. Brekelmans [b], M.G.D. Geers [b]

[a] *Corus Research Development and Technology, PO Box 10000, 1970CA IJmuiden, The Netherlands*
[b] *Faculty of Mechanical Engineering, Eindhoven University of Technology, PO Box 513, 5600MB Eindhoven, The Netherlands*

Received 21 April 2008; received in revised form 26 August 2008; accepted 12 September 2008
Available online 8 November 2008

Abstract

Thermal shock is a principal cause of catastrophic wear of the refractory lining of high temperature installations in metal making processes. To investigate thermal shock experimentally with realistic and reproducible heat transfer conditions, chamotte and corund refractory samples of ambient temperature were subjected to surface contact with molten aluminium followed by passive cooling in ambient air. The evolution of damage was characterized by measuring the transit time of ultrasonic longitudinal waves at various sample locations after each test cycle. The mechanical validity of transit time measurement was confirmed in independent experiments. The single test cycle performed with chamotte material indicated the reproducibility and reliability of the experimental set-up and damage characterization method. Multiple test cycles performed with corund material yielded a reliable set of data, to be used for model validation purposes. Both non-uniform damage due to temperature gradients as well as uniform damage due to exposure to a uniform temperature were determined experimentally. The interaction between both damage mechanisms requires further investigation as well as the possible shielding of heat transport by damage.

Keywords: Non-destructive evaluation; Mechanical properties; Thermal shock resistance; Refractories

1. Introduction

The refractory lining of iron and steelmaking installations is prone to wear as the result of excessive thermal stresses. This wear process occurs for example when molten steel is introduced into a cold ladle. Another example of this so-called thermal shock event is the sudden opening of an operating furnace where the hot refractory material becomes exposed to ambient air.

Experimental investigations into thermal shock behaviour of refractory materials are reported extensively in the literature. Severe down-quenching was achieved using water,[1–13] oil[14–17] and molten salt.[18] Milder down-quenching was realized using passive or active cooling by ambient air mostly preceded by mild up-quenching in a hot furnace atmosphere.[19–24] Also fluidized beds with ambient air were used for this purpose.[25] Severe up-quenching was achieved using burners,[26–29] molten metal,[30–32] lasers[33–35] and film heaters.[36] For this purpose also electrical induction,[37] resistance[38] and discharge[39] have been used on refractories containing carbon. Milder up-quenching was achieved using a hot furnace atmosphere,[40–43] infrared heaters[44] and hot compressed gas.[45] Due to the poor reproducibility of the heat transfer conditions most of the aforementioned test methods do not qualify for the use in a model parameter estimation process. A down-quenched sample in water is, e.g. surrounded by boiling water affecting the heat transfer. Lasers do provide a constant heat flux but only over a very small sample surface, not suitable for refractory material with coarse grains. Furthermore, the use of molten salts can lead to chemical corrosion. The up-quench achieved with a hot furnace atmosphere is of low severity and not representative for thermal shock in the refractories of interest here under realistic process conditions. Although up-quenching with burners does represent the heating of a process furnace, the heat flux generated is not constant over the sample surface.

Experimental characterization of thermal shock damage has been performed, e.g. by (microscopic) examination of the crack pattern,[18,28,31,33–35,45] recording the number of test cycles or the quenching temperature difference to reach material failure,[1,2,32] by determination of the residual

* Corresponding author.
E-mail address: erik.damhof@corusgroup.com (F. Damhof).

0955-2219/$ – see front matter © 2008 Elsevier Ltd. All rights reserved.
doi:10.1016/j.jeurceramsoc.2008.09.010

mechanical properties[1,3–5,8–10,25,36–39,42] and of the weight loss after layer-wise spalling.[43] Other characterization techniques rely on the measurement of acoustic emission during thermal shock[11,22,24,26,44,46,47] and the determination of the change in sound velocity,[40,48,49] attenuation[48] and resonance frequency[6,16,20,29] due to thermal shock. The described methods characterize the material state of an entire test sample and thus only allow for a qualitative ranking of materials. Apart from laborious and expensive techniques as X-ray and ultrasonic tomography,[50–52] the location-dependent characterization of damage evolution in coarse granular materials has not been reported yet.

Thermal shock initially induces micro-cracks, localizing to macro-cracks, depending on the load severity and repetition. To predict this thermo-mechanical behaviour a phenomenological constitutive model has been developed[53] based on Hooke's law for damaged isotropic material[54]:

$$\sigma = (1 - D)\,{}^4\mathrm{C} : \varepsilon_{el} \tag{1}$$

with σ the stress tensor, D a scalar variable representing the damage ranging from zero to unity (loss of structural integrity), ${}^4\mathrm{C}$ the fourth order elasticity tensor of the undamaged material and ε_{el} the elastic strain tensor, which is here induced by a constrained thermal expansion. The damage D includes both non-uniform and uniform damage. Thermal shock leads to temperature gradients, non-uniform thermal expansion and non-uniform damage. A uniform temperature increase induces uniform thermal expansion in mechanically unconstrained configurations. This may lead to uniform damage due to micro-scale thermal expansion mismatches within the microstructure of the material.[55–57]

Damage development is described by evolution laws, involving material-dependent parameters. These have to be determined from standard tests and dedicated experiments reflecting the thermal shock damage process under consideration with representative and reproducible boundary conditions. Model parameter estimation requires furthermore the quantification of the evolution of damage at various locations in a test sample.

In this paper an experimental set-up is proposed allowing the triggering of a thermal shock with reproducible heat transfer conditions such that realistic process conditions are adequately represented. The damage evolution in a test sample, using consecutive test cycles, is characterized by measuring the transit time of ultrasonic longitudinal waves at various locations. The discussion starts with the specification of the test materials used and selected experimental details on the method of damage characterization. Thereafter quasi-stationary heating and cooling experiments are described to introduce the phenomenon of uniform thermal damage experimentally. In order to establish the mechanical validity of the damage characterization method a comparison is made between the residual mechanical and the corresponding acoustic damage properties after water quench experiments. The thermal shock experiments discussed subsequently entail the surface contact of ambient refractory samples with molten aluminium followed by cooling in ambient air. To simulate the one-dimensional temperature profile of thick-walled refractory linings of high temperature installations, thermal insulation is applied at the non-quenched sample sides. Reproducible damage evolution was measured in two different types of refractory material and a representative set of data was obtained, useful for future model validation purposes.

Table 1
Chemical composition of the test materials.

	Rel. weight of components (%)	
	Chamotte	Corund
Al_2O_3	58.7	90.9
SiO_2	40.0	8.8
Na_2O	–	0.2
Fe_2O	1.1	–

2. Materials

Chamotte and corund refractory materials have been used in the experiments presented in this paper. Chamotte material is typically applied in the shaft of a blast furnace suitable for the production of raw iron and in iron and steel ladles. Corund material is typically used in the hearth of a blast furnace, in re-heating furnaces of a hot strip mill plant and in reactor vessels used in the petro-chemical industry. The test materials have been selected for their known sensitivity to thermal shock. Samples were cut to size from commercially available refractory bricks. The chamotte bricks, based on a combination of calcined clays (chamotte) and raw clays, received their final properties after pressing and drying during a sintering stage of 15 h in a tunnel kiln heated to a temperature of 1400–1450 °C. The corund bricks, based on corundum and mullite, received their final properties after pressing and drying during a sintering stage of 3–5 h in a tunnel kiln heated to a temperature of 1500–1600 °C. The chemical composition of both materials is presented in Table 1. The main properties at room temperature are presented in Table 2, as well as characteristics reflecting the material structure.

With the presented material properties the Hasselman parameter R for resistance against thermal shock fracture initiation[58]

Table 2
Properties of the test materials.

Property	Symbol	Unit	Chamotte	Corund
Density	ρ	$\mathrm{kg\,m^{-1}}$	2220	3038
Porosity	ϕ	%	18.2	17.0
Young's modulus	E	GPa	10.0	13.0
Poisson's ratio	ν		0.22	0.22
Bending strength	σ_2	MPa	9.0	8.7
Compressive strength	σ_c	MPa	27.8	68.9
Thermal expansion	α	$\mathrm{K^{-1}}$	6×10^{-1}	8×10^{-1}
Thermal conductivity	χ	$\mathrm{W\,m^{-1}\,K^{-1}}$	2.0	3.7
Thermal capacity	C_2	$\mathrm{J\,kg^{-1}\,K^{-1}}$	788	773
Maximum grain size	–	mm	3	4
Average grain size	–	mm	2	3

defined by

$$R = \frac{\sigma_b(1-\nu)}{\alpha E} \quad (2)$$

can be determined. The parameter R represents the maximum allowable temperature increase in a material during infinitely fast heating-up. For the chamotte and corund sample materials this parameter values 117 °C and 65 °C, respectively. The predicted allowable temperature increase is largely exceeded in the thermal shock tests discussed in this paper. This implies that considerable damage can be expected.

3. Damage characterization

The characterization of damage in the test samples is performed by measuring the transit time of ultrasonic longitudinal waves using a Pundit system from C.N.S. Farnell. The exciting and receiving transducers are located on the tests samples opposite to each other. Hence, the wave propagation direction is perpendicular to the transducer surfaces. The average longitudinal wave velocity V is determined as the ratio of the distance between the transducers and the transit time. Subsequently the dynamic Young's modulus E_{dyn} is calculated according to:

$$E_{dyn} = \rho \left[\frac{(1+\nu)(1-2\nu)}{(1-\nu)}\right] V^2 \quad (3)$$

Damage, as a result of micro-cracks induced by, e.g. thermal shock, increases the wave transit time and consequently causes a reduction of E_{dyn}. The relative decrease of this dynamic modulus with respect to the initial (undamaged) state is defined in this paper as the damage D, unless mentioned otherwise. The density and Poisson's ratio are assumed to be only negligibly affected by damage.

In the experiments reported in this paper, transducers of 54 kHz (40 mm diameter) have been used for the larger samples and transducers of 200 kHz (20 mm diameter) have been used for the smaller samples and for location-dependent measurements. Similar results were obtained with both transducer types. For a typical refractory wave velocity of 3200 m/s wave lengths (calculated from the ratio of velocity and frequency) of 0.059 m and 0.016 m are thus generated, respectively. In the context of the maximum grain size of the refractory materials investigated, see Table 2, the spatial resolution is fully acceptable.

The acoustic contact between the transducers and the test samples is established by applying 1 mm thick self-adhering silicon rubber pads to the transducers. The registered transit time has to be corrected with that of the rubber pads which was determined in dedicated experiments. In the 'sandwich experiments' described hereafter contact gel was used to establish the acoustic contact between the samples and transducers but also between individual samples.

To investigate how non-uniform damage may affect the wave transit time the latter was measured over two 'sandwiches', composed of pairs of refractory samples: 1 and 2 in series as well as 3 and 4. Samples 1, 3 and 4 (height/transducer distance 30 mm) were of corund material. Sample 2 (height/transducer distance 50 mm) was of chamotte material. Contact gel was used for acoustic coupling with the 200 kHz transducers and between the individual sandwich components. It is assumed here that the contact gel neither penetrated the sample surfaces nor affected the transit time. The transit time was measured of both the sandwiches and their individual components. Subsequently all the relevant material surfaces were polished (using 120 diamond followed by 1200 diamond disks) and the measurement was repeated.

Table 3
Results of the sandwich experiments.

Sample no.	Unpolished		Polished	
	Transit time (μs)	Height (mm)	Transit time (μs)	Height (mm)
1	9.5	30.34	9.4	30.01
2	15.7	50.03	15.4	49.71
1 + 2 individual	25.2	80.37	24.8	79.72
1 + 2 sandwich	25.6	80.37	24.8	79.72
3	6.3	30.31	6.1	29.65
4	6.7	30.36	6.5	29.92
3 + 4 individual	13.0	60.67	12.6	59.77
3 + 4 sandwich	13.4	60.67	12.6	59.77

Table 3 presents the results of the sandwich experiments. It can be observed that the transit times of the polished sandwiches are equal to the summed transit times of their individual components. The difference of 0.4 μs appearing when dealing with the unpolished samples is ascribed to the roughness of the relevant sample surfaces. These results indicate furthermore that in case of non-uniform damage, the measured transit time equals the summed transit time of the various damaged material zones present between the transducers.

Polishing of the samples lowers the transit time with 1–3% and 2% for the measurements with 30 mm and 50 mm transducer distance, respectively. Given these low percentages and the common scattering in material properties of coarse grained refractory materials, the effect of surface roughness will be neglected in the rest of this paper.

4. Uniform damage experiments

The effect of a uniform temperature field on refractory material was investigated by subjecting corund samples to quasi-stationary heating and subsequent cooling. The resulting acoustic damage was compared with the residual crushing strength.

4.1. Experimental set-up and procedures

Cube-shaped corund samples with sides of 50 mm are placed in a furnace and are heated quasi-stationary up to a range of temperatures. Except for the ultimate corner areas this symmetric sample geometry promotes the induction of a uniform temperature field after a dwelling period the samples are cooled down quasi-stationary to ambient temperature. Maximum furnace temperatures of 450 °C, 600 °C, 750 °C and 900 °C have been applied, which are within the temperature range of the

Table 4
Experimental programme for uniform damage tests.

1	Measure transit time, determine E_{dyn}
2	Heating at 2 °C min
3	Dwelling at maximum temperature for 120 min
4	Coding at 2 °C min
5	Measure transit time, determine E_{dyn} and damage
6	Perform ambient crushing test, determine crushing strength

thermal shock experiments described in Sections 5 and 6. For each temperature level, three samples have been used. To determine the damage both the 54 kHz and 200 kHz transducers were used for transit time measurements with similar result. As their diameter better suited the sample size and the expected uniform damage field only the results obtained with the 54 kHz transducers are dealt with in the following. These transducers were positioned at the opposite face centers of the sample. This resulted in three mutually orthogonal measurements per sample. After the thermal treatment the samples were subjected to room temperature crushing tests. The nominal crushing strength was determined as the maximum load divided by the virgin sample area. Table 4 presents the detailed test programme.

4.2. Results

Fig. 1 (left) presents the average batch damage as a function of the maximum temperature as well as the residual crushing strength of the individual samples as function of their dynamic Young's modulus determined after the thermal treatment. The trend lines are obtained from linear regression. The damage induced by the uniform temperature field appears to be linearly depending on the maximum temperature. As the attained testing temperatures do not exceed the maximum sintering temperature used in the processing of the refractory materials the occurring damage originates solely from thermal expansion mismatches within the microstructure of the material. Moreover, the material constituents are such that thermo-chemical changes at temperatures below the sintering temperature are not expected.

Only a moderate correlation appears to exist between the residual crushing strength and E_{dyn}, determined after the thermal treatment, as shown in Fig. 1 (right). The observed large statistical variations in the crushing strength, characteristic for coarse grained materials hampers definite conclusions. The closure of the micro-cracks present, prior to reaching the material failure state may also contribute to this moderate correlation. The material degradation determined with ultrasonic measurements is only weakly confirmed here by a deteriorating crushing strength. Nonetheless in recently published work[49] a relation between the degrading strength of refractory material in compression due to thermal shock and the corresponding degradation in ultrasonic longitudinal sound velocity has been observed.

5. Thermal shock experiments with hot air followed by water quenching

The proposed damage characterization method is validated mechanically by comparing the residual bending strength with the acoustic damage in samples subjected to water quench experiments.

5.1. Experimental set-up and procedures

To induce an up-quench thermal shock under mild conditions, beam shaped corund samples of ambient temperature and of dimensions 30 mm × 30 mm × 150 mm are inserted rapidly into a furnace, which was pre-heated to a temperature of 1200 °C.

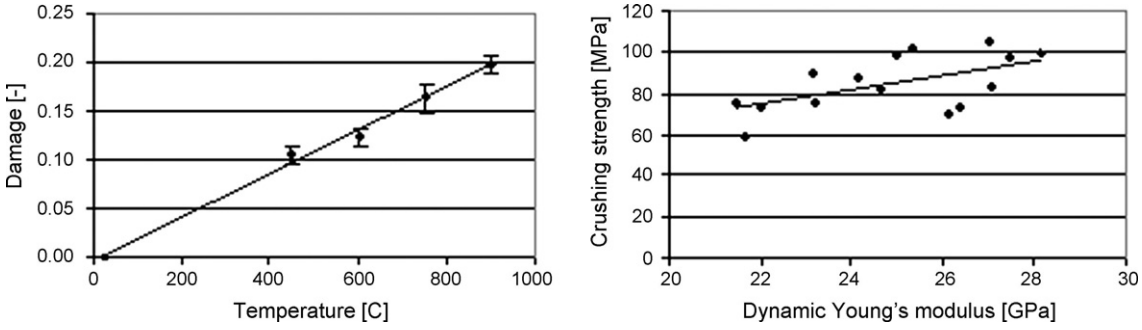

Fig. 1. Uniform damage (left) and residual crushing strength (right).

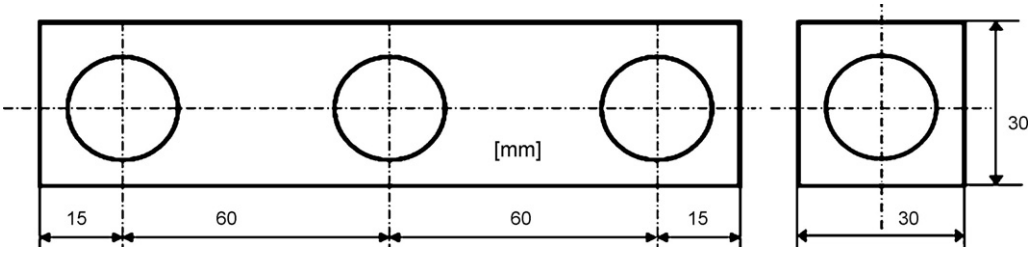

Fig. 2. Measurement grid (200 kHz transducers) used in the non-uniform damage test.

After a dwelling period to allow redistribution to a uniform temperature, the samples are quenched in silent water of ambient temperature. A large volume of water was used to maintain a constant bath temperature during the down-quench.

The damage was determined from transit time measurements using the 200 kHz transducers at the locations depicted in Fig. 2. Acoustic measurements were performed at three sample locations in the two perpendicular transverse directions as well as centrally in the longitudinal direction. This results in seven measurements per sample.

The experiment started with a series of 18 samples. After each test cycle three samples were removed from the series and subjected to a three-point bending test. Also a separate set of three virgin samples was subjected to a three-point bending test without receiving the thermal treatment. The bending strength was determined from the maximum load and the geometrical bending properties of the sample cross-section. The detailed test programme is presented in Table 5.

Table 5
Experimental programme for water quench tests.

Start with batch of 18 samples
1Measure transit time and determine E_{dyn}
2Introduce samples into heated furnace of 1200 °C
3Dwelling time of 60 min in the furnace
4Quench samples in ambient silent water
5Dry samples for 60 min at 110 °C
6Measure transit time, determine E_{dyn} and damage
7Remove three samples from batch and subject these to three-point bending test
8Determine bending strength of these three samples
Repeat steps 2–8 with the remaining samples

5.2. Results

Fig. 3 shows the average transversal and longitudinal damage determined from transit time measurement (left) and the residual bending strength (right) as function of the number of test cycles. The introduced mechanical damage variable D_b represents the relative decrease of the residual bending strength compared to the bending strength of the undamaged batch (10.28 MPa). With the effective stress concept[54] it can be shown that the damage defined by D_b is mechanically equivalent with the damage conventionally based on the degradation of the elastic stiffness properties. It can be observed that the largest increase in acoustic as well as in mechanical damage is obtained in the first three thermal shock cycles. The damage saturates in the consecutive test cycles which might be due do the increasing density of the network of micro-cracks with the number of thermal shock cycles. This implies that the available energy, per test cycle, for the propagation of each micro-crack, decreases in the consecutive thermal shocks.

Qualitatively the average transverse and longitudinal damage exhibit a similar dependency on the number of thermal shock cycles. The higher damage in the longitudinal direction is attributed to the beam shaped sample geometry. The shrinkage of the sample in the water quench experiments induces a preferential direction of the micro-cracks, perpendicular to the

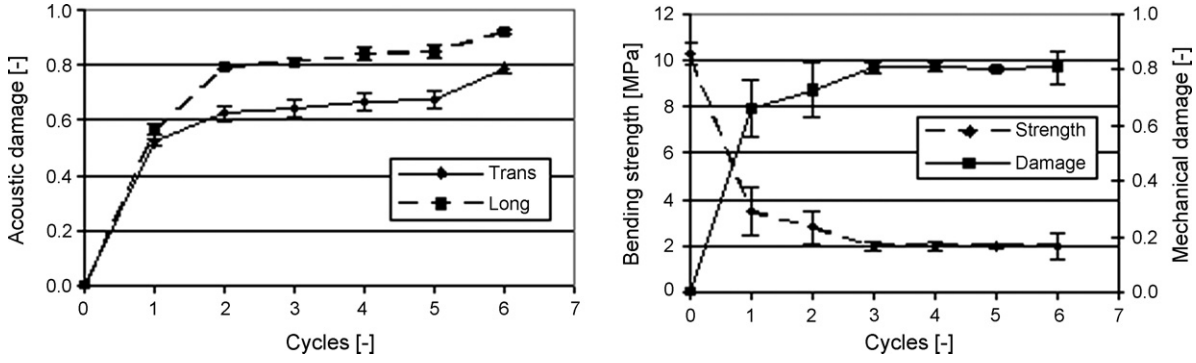

Fig. 3. Acoustic (left) and mechanical damage (right) after cycling.

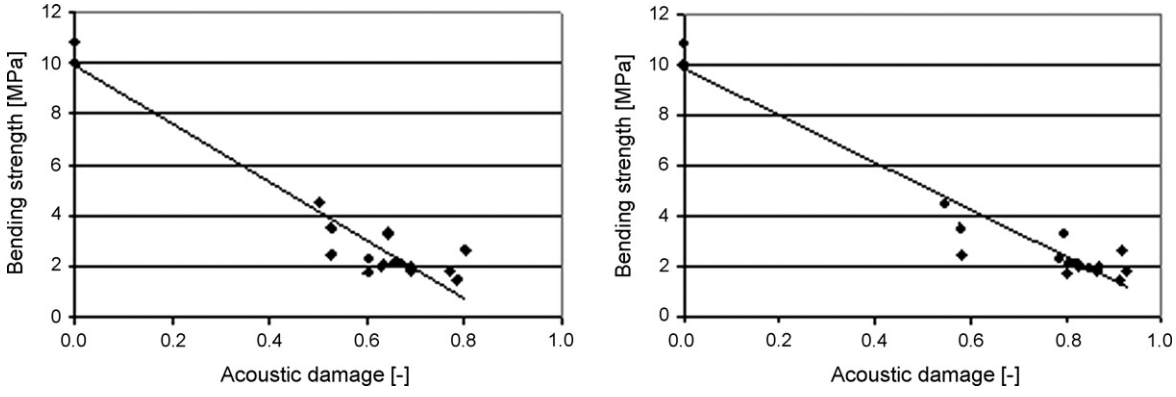

Fig. 4. Bending strength versus transversal (left) and longitudinal damage (right).

longitudinal sample axis. Fig. 3 shows that indeed the longitudinal damage compares better with the damage variable D_b than the transversal damage.

Fig. 4 presents the (residual) bending strength of the individual samples as function of the acoustic transversal damage (D_{trans}) and longitudinal damage (D_{long}). It can be observed that both damage indicators have a predictive value with regard to the degradation of the bending strength as a result of the applied thermal treatment. From a theoretical point of view, it is expected that the strength vanishes when the damage approaches unity. This is particularly the case for the longitudinal damage which again confirms its predictive value. The qualitative equivalence between D_b and D_{long}, presented in Fig. 3, as well as the observed correlation between the bending strength and the acoustic damage, presented in Fig. 4, underline the quantitative correlation between the defined damage indicators and the static damage. The latter is defined as the relative decrease of Young's modulus, determined from mechanical tests, compared to the initial, undamaged state. This static damage is typically used in constitutive models describing damage evolution.[53,54] For the future experimental validation of such models it appears that a direct comparison can be made between the numerically calculated damage and the damage obtained from transit time measurements.

In general, thermal shock induces damage caused by tensile failure at the micro-scale. Assuming that material failure in bending proceeds accordingly, the results depicted in Figs. 3 and 4 indicate that transit time measurement of ultrasonic longitudinal waves provides an adequate and reproducible way to characterize the evolution of thermal shock damage.

6. Thermal shock experiments with molten aluminium

To simulate thermal shock with realistic and reproducible boundary conditions, representative for metal making processes, refractory samples of ambient temperature were brought into contact with molten aluminium followed by cooling in ambient air. Experiments with chamotte and corund material were performed to investigate the viability of the experimental set-up. The corund material was subject to multiple thermal shock cycles to induce damage evolution and to produce a reliable set of data for future model validation.

6.1. Experimental set-up and procedures

Solid aluminium is molten and heated to 1000 °C in an open induction furnace, powerful enough to maintain a constant bath temperature. A guiding system, mounted on top of the furnace, enables an accurate and fast positioning of the test samples on top of the aluminium bath, minimizing the heating-up by radiation. Prior to this the aluminium bath was stirred to remove any oxidation layer present and to safeguard the thermal contact between bath and sample. The set-up is shown schematically in Fig. 5. After surface contact with the aluminium bath for a period of time, the samples were removed from the set-up and cooled in ambient air, inducing a down-quench thermal shock. According to the calculated Hasselman parameter R of the sample materials the imposed difference of initial sample and bath temperature is high enough to induce thermal shock damage.

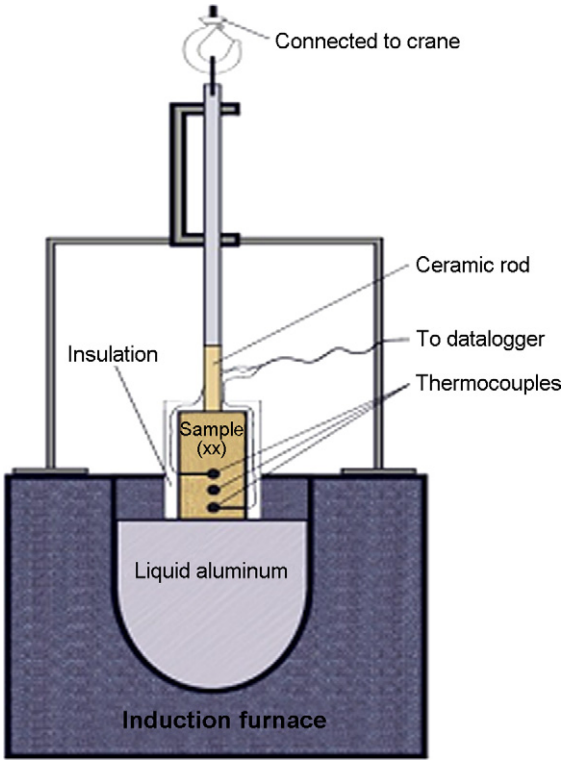

Fig. 5. Thermal shock test set-up.

A number of three chamotte and six corund samples of dimensions 50 mm × 50 mm × 150 mm were used. The temperature was measured in two corund samples (1 and 2). From the other corund samples (3–6) and from the chamotte samples the damage was determined.

Apart from the quenched surface (50 mm × 50 mm) all sample sides were cladded with 30 mm thick thermal insulation. This triggers a one-dimensional temperature profile similar to that encountered in thick-walled refractory linings of high temperature installations. Terracoat® was applied at the quenched sample side to prevent invasion of the molten aluminium.

During the experiment the temperature was measured and recorded as a function of time of samples 1 and 2 of the corund material. To this end thermocouples were mounted on the longitudinal axis of the samples, at distances of 10 mm, 25 mm and 40 mm from the quenched sample side. To minimize the effect on the temperature profile, the holes for the thermocouple wires were drilled orthogonally as illustrated schematically in Fig. 6. This figure also shows the ceramic tube, inserted over a length of 40 mm in the sample for the connection with the guiding system.

With each of the chamotte samples a single thermal shock cycle was performed. The corund samples were subject to three consecutive thermal shock cycles (indicated as C1, C2 and C3) in order to investigate the evolution of thermal shock damage. After a period of 20 min surface contact with the molten aluminium a hold time of 48 h was maintained to allow the complete cooling down of the samples. Consecutively, the insulation material was removed from the chamotte samples and from the corund

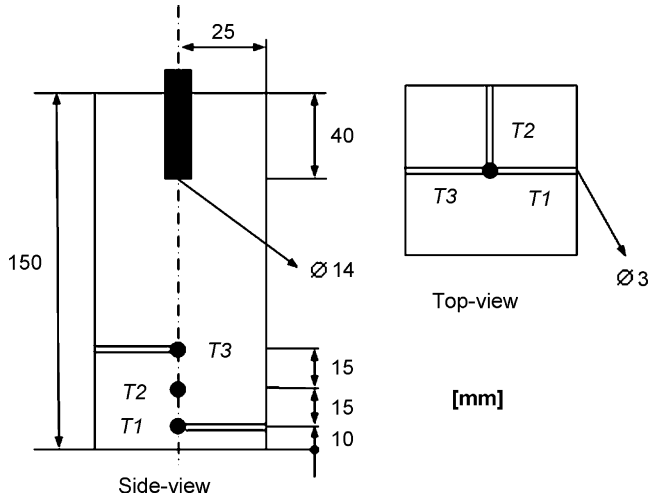

Fig. 6. Corund sample with thermocouple locations and wire feeds.

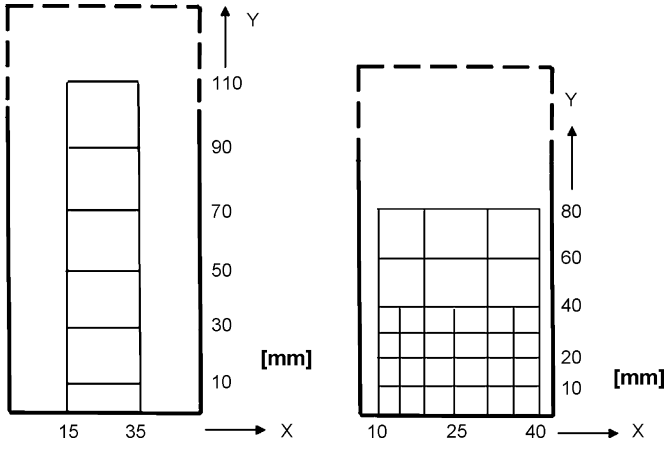

Fig. 7. Measurement grid for chamotte (left) and corund sample (right).

samples 3–6. Transit time measurements were then performed at various locations on these samples. This was also done prior to the first thermal treatment. The 200 kHz transducers were positioned at the locations coinciding with the line intersections in the measurements grids schematically illustrated in Fig. 7.

Table 6
Experimental programme for one-sided thermal shock tests with corund samples.

1	Measure transit time, determine E_{dyn} of samples 3–6
2	Surface contact of samples with molten aluminium of 1000 °C for 20 min. Register temperature of samples 1 and 2
3	Cool down samples in ambient air for 48 h. Continue temperature registration of samples 1 and 2 for 30 min
4	Measure transit time, determine E_{dyn} and damage of samples 3–6 Repeat steps 2–4 tuyice

Compared to the chamotte material the grid used for the corund material was of higher density as these results are to be used for quantitative model validation in the furnace. The transit time measurements were performed between the opposite pairs of sample faces in the two orthogonal directions. In the processing of the results it is assumed from theoretical considerations that the experimental damage will be symmetric with respect the longitudinal sample axis. The damage after each thermal shock cycle was calculated as the relative decrease of the corresponding residual E_{dyn} compared to the value in the undamaged state. The detailed test programme with the corund samples is presented in Table 6.

6.2. Results

6.2.1. Chamotte material

Fig. 8 (left) presents the damage determined in an individual chamotte sample. The orthogonal pairs of sample surfaces on which the acoustic measurements are performed are denoted by AA and BB. It can be observed that the single thermal shock cycle has induced significant damage in the sample. Despite the scattering in damage at a given Y-coordinate the trend of an increasing damage with a decreasing distance to the molten aluminium is noticeable. The observed scattering in the results is ascribed to the common variation in material properties of refractory bricks due to processing and their heterogeneous granular structure.

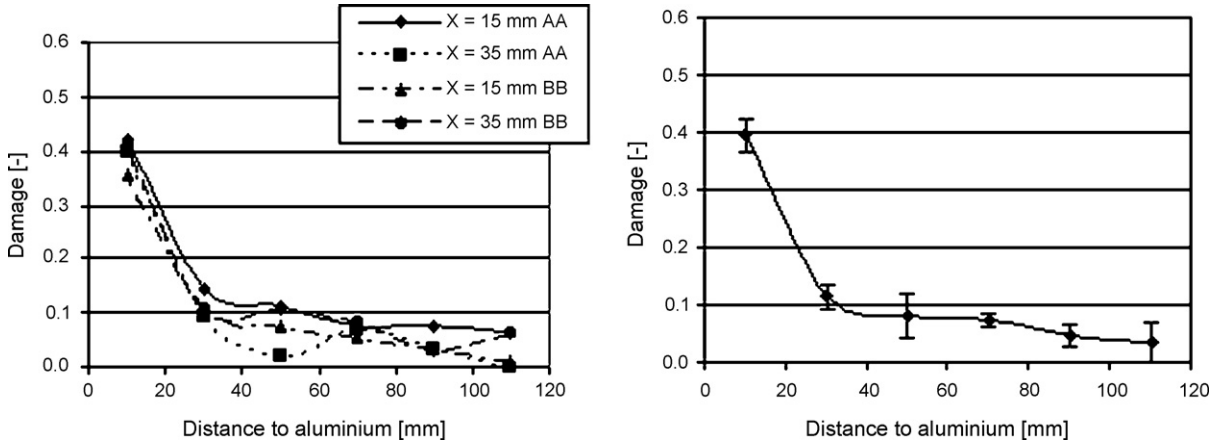

Fig. 8. Damage in an individual chamotte sample (left) and averaged over all coordinates and all samples (right) (AA and BB denote orthogonal measurement directions).

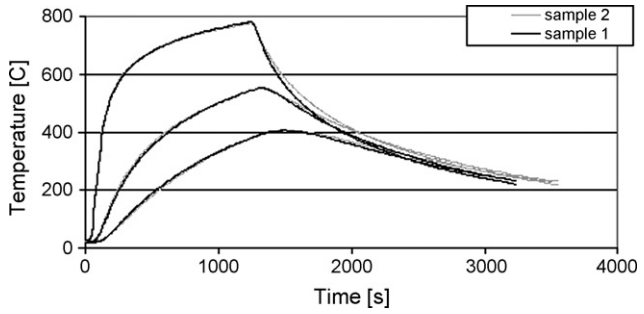

Fig. 9. Temperatures in corund samples 1 and 2 during the first test cycle.

The damage averaged over all X-coordinates, at a given Y-coordinate of all chamotte samples used, is presented in Fig. 8 (right). The use of three test samples and four transit time measurements per sample at a given Y-coordinate results in an average of 12 transit time measurements per data point. It can be concluded that with the presented experimental set-up the damage can be effectively created while the characterization method renders a reproducible quantification.

Fig. 8 (right) shows that most damage is concentrated in the vicinity of the quenched sample side where the temperature gradients are the highest. At 10 mm distance from the molten aluminium a damage level of 0.39 is achieved. This may be exceeded by even higher damage levels at smaller distances from the quenched sample side. From a macroscopic mechanical point-of-view this is unlikely. The thermal expansion at the heated, quenched sample side induces a compressive stress state equilibrated somewhat higher in the sample by a state of tensile stress. The latter induces tensile strains exceeding the material limits and causing the initiation of damage at some distance from the quenched sample surface. Nonetheless at distances to the molten aluminium smaller than 10 mm, thermal expansion mismatches at the microscopic level may induce micro-cracks and damage. Here appropriate transit time measurements could not be performed given the 20 mm diameter of the transducers used.

Lower thermal gradients will be present higher in the sample where uniform, thermal damage might be more prominent. Contributions to the observed damage may also originate from phase changes in certain constituents (e.g. SiO_2) of the sample material. This can be accompanied by local volume changes and thermal expansion affecting the transit time of passing ultrasonic waves and E_{dyn} determined thereof.

6.2.2. Corund material

Fig. 9 presents the temperatures $T1$, $T2$ and $T3$ (see Fig. 6) of corund samples 1 and 2 measured in test cycle 1. A good reproducibility of the temperatures can be observed indicating a reproducible heat transfer to and from the samples in respectively the heating and cooling cycle. Nonetheless sample 2 seems to cool down somewhat slower. This could be due to residues of aluminium, attached to the quenched sample side and affecting the irradiative heat transport to the ambient surroundings.

Evidently, the thermocouple temperature $T1$ near the quenched sample side exhibits the steepest increase over time. At that location the highest temperature gradients and thermal shock appear. The temperature at which the maximum temperature rates occur lies below 300 °C, a temperature area in which

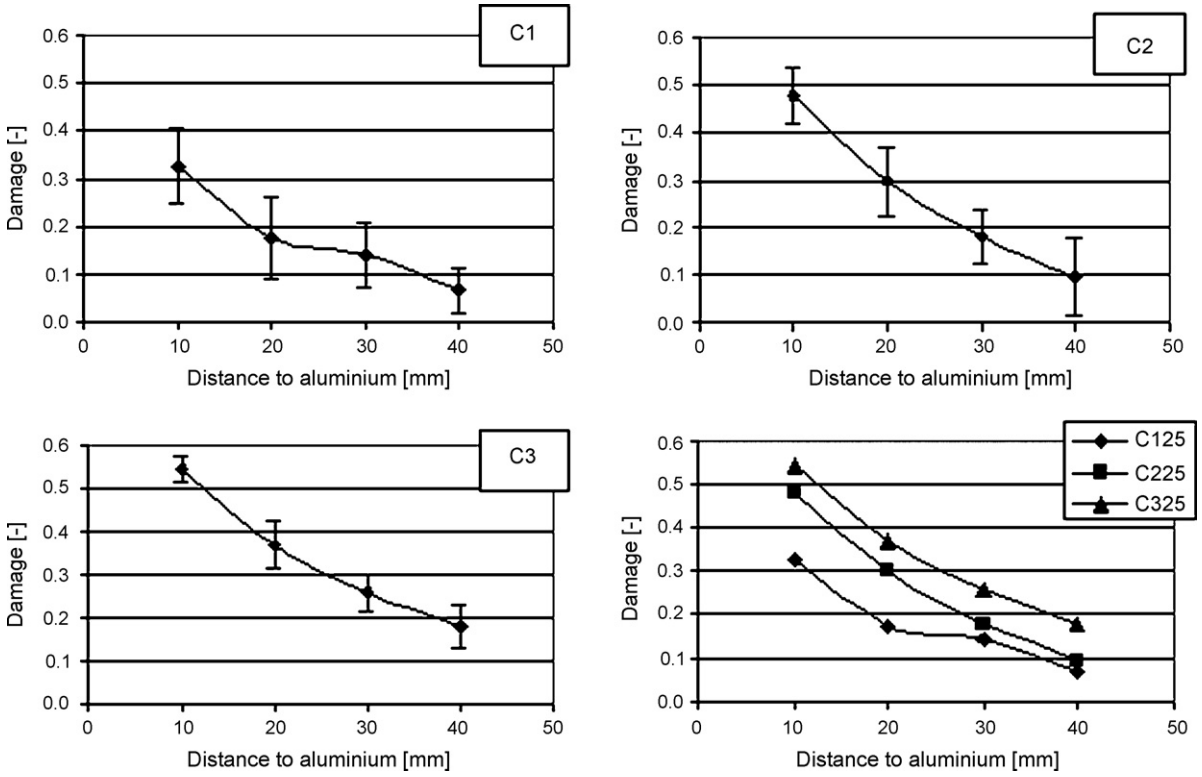

Fig. 10. Damage in the corund samples at the 25 mm X-coordinate (sample axis).

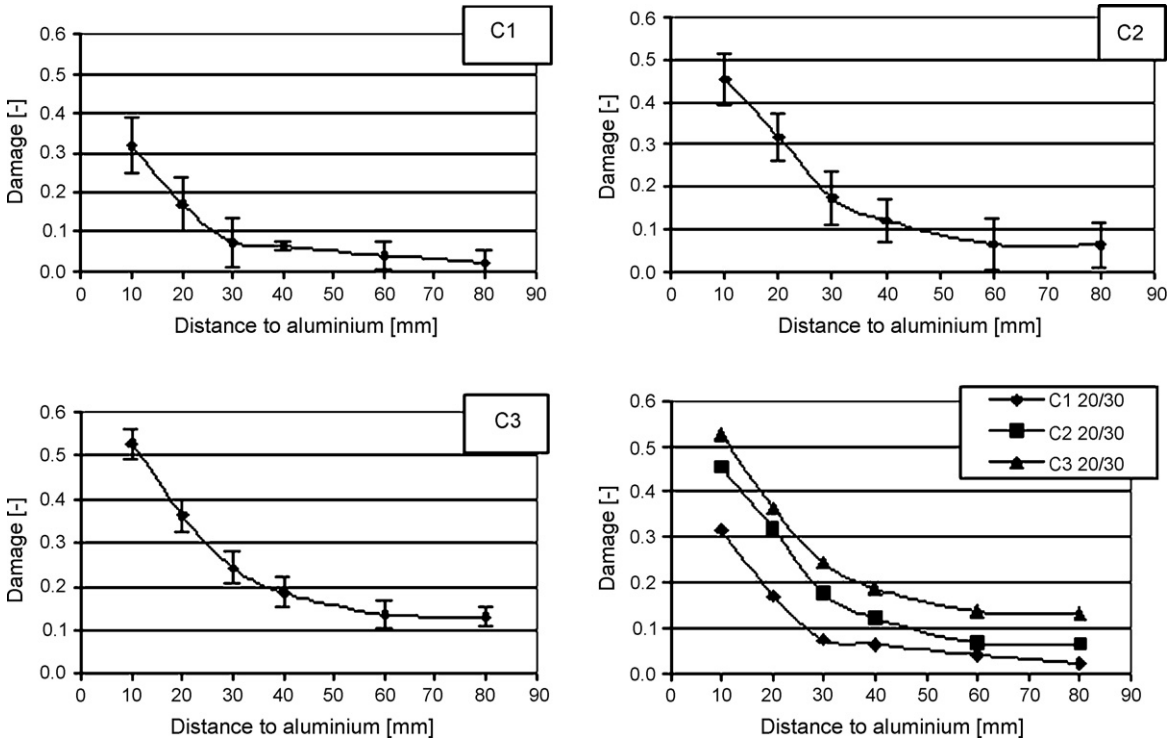

Fig. 11. Damage in the corund samples at the 20/30 mm X-coordinate.

the properties of the corund sample material do not change. The temperatures $T2$ and $T3$ at positions 25 mm and 40 mm still rise after the onset of the cooling period. At these locations the heat flow is still directed from the molten aluminium into the sample. At even higher locations the temperature might continue to rise during the first half hour of the cooling period. Uniform thermal damage may be more dominant there as the temperature rates will remain relatively low.

Figs. 10–13 present the average damage distribution in the corund samples 3–6 in the three consecutive test cycles C1

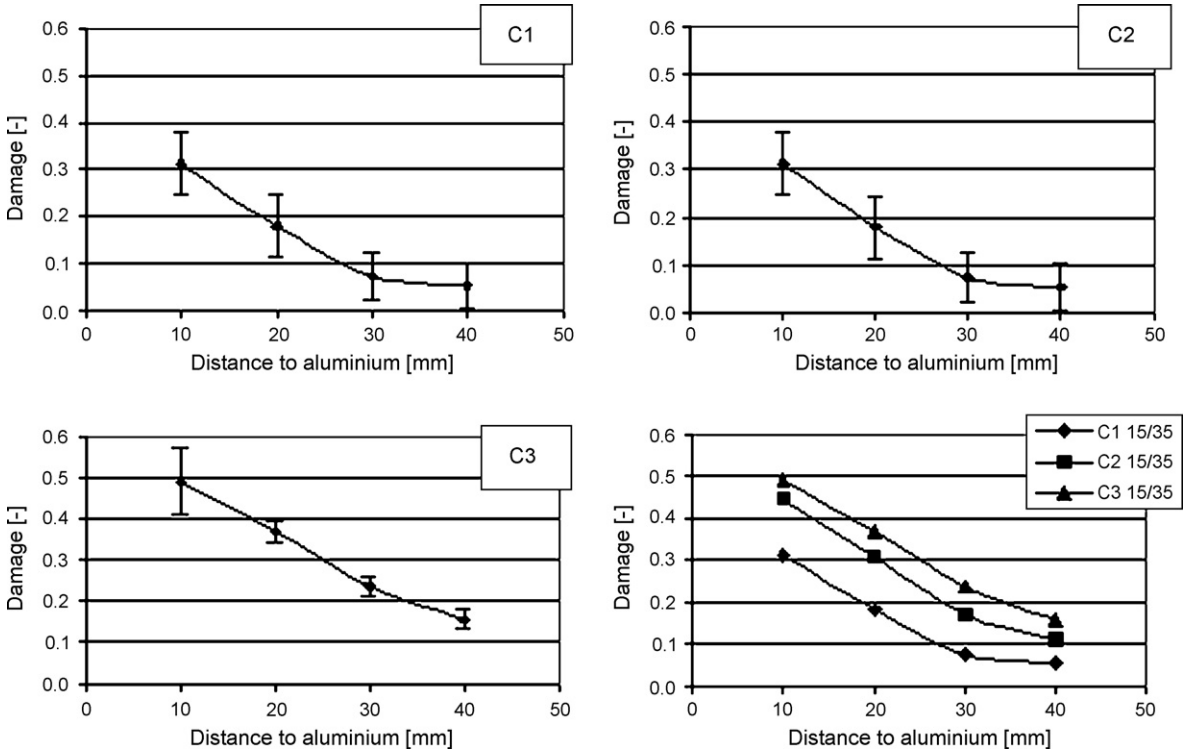

Fig. 12. Damage in the corund samples at the 15/35 mm X-coordinate.

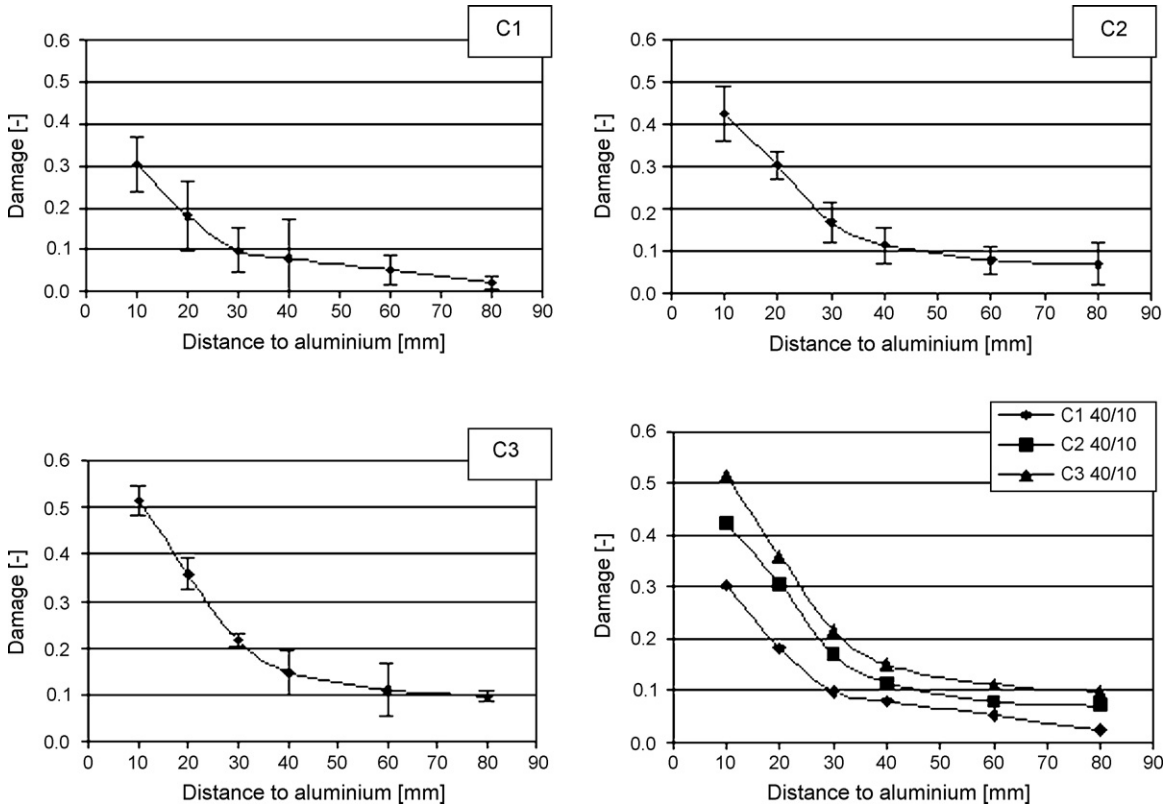

Fig. 13. Damage in the corund samples at the 10/40 mm X-coordinate.

to C3. The damage depicted is the average value of the pairs obtained at the X-coordinates (see Fig. 7 (right)) 20 mm and 30 mm, 15 mm and 35 mm as well as 10 mm and 40 mm. As the transit time measurements were performed on the two pairs of orthogonal sample faces on a batch consisting of four samples the presented data points are obtained from averaging over 16 sets of data. It is again assumed here that the sample geometry induces a symmetric damage pattern with respect to the longitudinal sample axis. Analogically the data points at the 25 mm X-coordinate (sample axis) are obtained from averaging over eight sets of datas. It can be observed that the set of data depicted represents the damage evolution in the sample material in a reasonably reproducible way. The exposure of the samples to multiple consecutive thermal shock cycles has lead to a reproducible damage at various locations along the sample height. This confirms the homogeneity of the sample material with regard to the determined acoustic stiffness properties in damaged and in undamaged state. It appears furthermore that the damage pattern determined at the X-coordinates 10 mm and 40 mm was not influenced by edge effects and surface roughness resulting from possible damage caused by cutting the samples to size.

As predicted by the low allowable value of the governing Hasselman parameter R, the corund sample material will be affected by damage due to the sudden heat input induced by the repeated surface contact with the molten aluminium. Thermal conduction and forced convection due to flowing of the molten aluminium in the induction furnace both contribute to the heat transfer in the up-quench stage. Compared to the cooling stage, characterized by radiation and free convection, this results in a high heat transfer coefficient and corresponding thermal gradients. The difference in temperature rates at the beginning of the heating and cooling period can be observed in Fig. 9. At, e.g. the 25 mm X-coordinate maximum damage levels of 0.32, 0.48 and 0.53 were obtained in the consecutive thermal shock cycles C1 to C3, respectively. In all test cycles the damage decreases rapidly with increasing distance to the aluminium contact area. The fact that a uni-axial thermal load is applied, is reflected in the damage which does not vary significantly between the X-coordinates for a given Y-coordinate.

The evolution of damage is the highest in the first thermal shock cycle. Analogically to the previously discussed water-quench tests, the damage is saturating in the consecutive test cycles. In view of the constant temperature of the aluminium bath the heat input in the consecutive test cycles is invariant although the damage increases considerably. This cannot be attributed to a uniform damage development as the maximum temperature is already achieved in the first test cycle. Apparently with every test cycle the sample material becomes increasingly susceptible to further damage propagation. With regard to the considerable damage increase at particularly the X-coordinates 60 mm and 80 mm this effect may be amplified by shielding of the heat transport by the micro-cracks present. The degraded thermal conductivity then induces higher thermal gradients in the material and more non-uniform damage. When the insulated test sample is considered as a semi-infinite wall an approximation of the penetration depth d of a sudden heat pulse can be derived from the governing analytical solution for the

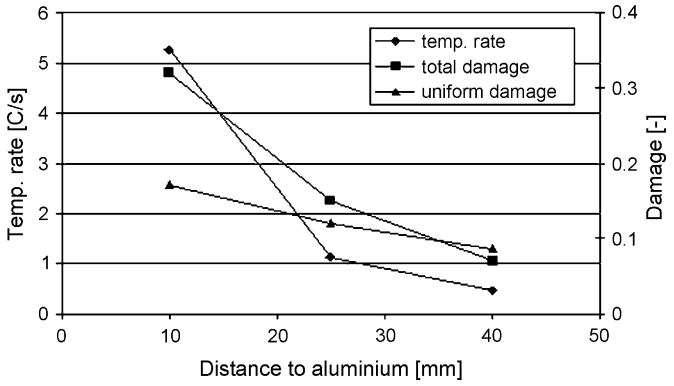

Fig. 14. Temperature rates and damage in corund samples at the thermocouple positions.

temperature distribution[59] and reads:

$$d = \sqrt{\pi \frac{\lambda}{\rho C_p} t} \tag{4}$$

with t the time period of surface contact with the molten aluminium. The penetration depth is then estimated to be 7.7 cm, using the properties listed in Table 2. This indicates that at sample locations as high as the 80 mm Y-coordinate the achieved thermal gradients may be high enough to cause non-uniform damage. The occurring thermal gradients can be quantified more accurately with appropriate thermal models. This item is, however, not within the scope of this paper. It is finally stated that property changes at temperatures below the specified ultimate sintering temperature can only be of thermo-mechanical nature, according to the information supplied by the producer of the refractory bricks used.

Fig. 14 shows the damage at the 25 mm X-coordinate, after the first test cycle, compared at the thermocouple positions with the maximum occurring temperature rate as determined from Fig. 9. The damage at the 25 mm thermocouple position was obtained from averaging the damage determined at the 20 mm and 30 mm Y-coordinate. A prediction of the uniform damage at the thermocouple positions, has also been added. To this end, the trend line derived from the uniform damage experiments as presented in Fig. 1 (left), has been used. It can be observed that the temperature rates decline rapidly with increasing distance from the quenched sample surface. Yet, a temperature rate of 0.47 °C/s (28 °C/min) at the 40 mm thermocouple position is sufficient to induce thermal shock damage in the corund refractory material used. This implies that thermal shock also contributes to the damage present at even higher locations in the sample. Temperature rates as low as 0.17 °C/s (10 °C/min) suffice to cause non-uniform damage in the corund material used.

Fig. 14 reveals that the relative contribution of the uniform damage to the total damage increases with an increasing distance from the aluminium. Moreover, the predicted uniform damage exceeds the experimentally determined total damage at the 40 mm thermocouple position in a rather unphysical way. This is an indication that the development of uniform damage may be hampered by the development of non-uniform thermal shock damage. Both damage mechanisms may interact if in a certain material point the temperature as well as the temperature rate are increasing simultaneously. Similar to the observed damage saturation in consecutive thermal shock cycles the growth of uniform damage may also be shielded by the presence of non-uniform damage developed previously or vice versa.

7. Discussion

In high temperature installations the refractory bricks are surrounded by adjacent bricks and mortar joints imposing certain mechanical constraints. This influences the thermal shock behaviour to a degree where layer-wise spalling is prominent.[60,61] Although the heat transfer conditions in the one-sided quench tests are representative for thermal shock occurring in metal making processes, it is difficult to impose the aforementioned mechanical boundary conditions in a reliable and reproducible manner. The influence of such constraints on the exhibited thermal shock behaviour can, however be investigated with a numerical model which has to incorporate the constitutive damage behaviour representative for coarse grained refractory material.

The transit time measurements performed during the one-sided thermal shock experiments allowed the location-dependent characterization of damage evolution. Nonetheless the damage at a distinct location between the transducers cannot be quantified. This requires the use of a numerical damage model which can however be validated with the obtained set of data and subsequently be used to predict the damage at all distinct sample locations. The transit time measured, in case of non-uniform damage, is the cumulated transit time of the ultrasonic waves passing the various damaged material zones present between the transducers (Section 3). This facilitates the comparison with model predictions. The calculated damage in a material volume of finite dimensions can be recalculated into a representative transit time. Summation of such calculated transit times over the transducer distance yields a numerical simulation which can be compared with its experimental counterpart.

When a refractory material is subject to thermal shock the interaction between non-uniform and uniform damage may be of importance. This interdependency of both damage mechanisms can be investigated experimentally. Test samples, previously subjected to uniform damage experiments, can be subjected consecutively to thermal shock experiments or vice versa. However, if a temperature wave is travelling non-uniformly (i.e., via unstationary heat transport) through the material both non-uniform and uniform damage can develop simultaneously and may interact. In a material, sensitive to both damage mechanisms, this occurs when both the thermal gradients (non-uniform damage) and the temperatures (uniform damage) are increasing and have not yet reached their maximum values. This distinguishable effect on the mechanical behaviour is not reflected well by consecutive experiments involving both damage mechanisms and can only be investigated by indirect identification procedures, that rely on a parallel numerical description of the interaction phenomena. The following, frequently used relation accounts for the simultaneous interaction between non-uniform,

elastic and uniform, thermal damage[55–57]:

$$D = 1 - (1 - d_{el})(1 - d_{th}) = d_{el} + d_{th} - d_{el}d_{th} \quad (5)$$

where d_{el} and d_{th} represent elastic and thermal damage, respectively. When both damage mechanisms contribute to the evolution of the total damage Eq. (5) clearly shows that they affect one another.

The experimental results of the one-sided quench experiments indicate that the thermal conductivity of the corund material may be influenced by damage. Similar to the degradation of elastic material properties, the degradation of the thermal conductivity by damage could also be quantified as a function of the damage variable D. When damage is considered as a form of porosity, Loeb's equation[62] is useful. Here the thermal conductivity decreases linearly with the evolution of damage until a residual value is attained. The parameters in the damage-conductivity relation can be obtained from (room temperature) thermal conductivity measurements on samples previously subjected to uniform damage experiments.

The residual mechanical properties determined after the uniform damage and water quench experiments only showed a moderate reproducibility compared to that of the corresponding acoustic properties. The coarse grain structure of the refractory material causes a variation in the location of crack initiation and propagation and a corresponding variation in the resulting mechanical properties. These may be obtained alternatively using relations as proposed by Posarac et al.[49] and Aly and Semler[63] who relate the degradation of strength to a corresponding decrease in ultrasonic velocity, i.e., acoustic damage. (The strength of the undamaged material has to be determined in that case.)

8. Conclusions

In order to investigate the evolution of thermal shock damage in refractory materials, a new experimental approach has been proposed. In contradiction to previously described methods, the imposed reproducible heat transfer conditions are representative for thermal shock in high temperature installations in metal making processes. The exposure of chamotte and corund refractory material to molten aluminium followed by passive air-cooling-induced high temperature gradients and corresponding damage levels. After consecutive test cycles the evolution of damage in the corund samples could be quantified in a reproducible way by measuring the transit time of ultrasonic longitudinal waves at various sample locations. With independent experiments the mechanical validity of transit time measurement was established. Apart from the application of laborious tomographic methods the location-dependent quantification of damage evolution in heterogeneous, granular materials has not been described before in the literature.

In a refractory material subject to an unstationary temperature increase (thermal shock) both non-uniform and uniform damage can develop simultaneously and may interact. Non-uniform damage is induced by internally and externally constrained thermal expansion. Uniform damage is induced by thermal expansion mismatches in the microstructural constituents of the material. Internally constrained thermal expansion can be reproducibly induced with the proposed experimental set-up for one-sided up-quench. The investigation of externally constrained thermal expansion and its effect on the exhibited thermal shock damage as well as the interaction between uniform and non-uniform damage can only be sufficiently investigated using a numerical model which can however be validated with the produced set of data.

Although saturating, the growth of damage in the consecutive test cycles performed with the corund material is considerable. This indicates an increased susceptibility of the corund material to the growth of non-uniform damage with an increasing number of test cycles, possibly facilitated by the shielding of heat transfer by damage. Locally this may lead to a degraded thermal conductivity, higher thermal gradients and a corresponding higher level of non-uniform damage.

References

1. Wei, W. J. and Lin, Y. P., Mechanical and thermal shock properties of size graded MgO-PSZ refractory. *J. Eur. Ceram. Soc.*, 2000, **20**, 1159–1167.
2. Volkov, T. and Jancic, R., Prediction of thermal shock behavior of alumina based refractories, fracture resistance parameters and water quench test. In *Proceedings of CIMTEC 2002*, ed. P. Vincenzini and G. Aliprandi, 2003, pp. 109–116.
3. Ko, Y. C., Horng, W. H., Wang, C. H. and Chieh Teng, L. C., Fines content effects on the thermal shock resistance of Al2O3-Spinel Castables. *Chin. Steel Tech. Rep.*, 2001, **15**, 7–14.
4. Aksel, C., The effect of mullite on the mechanical properties and thermal shock behaviour of alumina-mullite refractory materials. *Ceram. Int.*, 2003, **29**, 183–188.
5. Cotterel, B., Sze, W. O. and Caidong, Q., Thermal shock and size effects in castable refractories. *J. Am. Ceram. Soc.*, 1995, **78**(8), 2056–2064.
6. Tonnesen, T. and Telle, R., Evaluation of thermal shock damage in castables by a resonant frequency and damping method. In *Proceedings of 49th Internationales Feuerfest-Kolloquium 2006*, 2006, pp. 133–136.
7. Anderson, T. and Rowcliffe, D. J., Thermal cycling of indented ceramic materials. *J. Eur. Ceram. Soc.*, 1998, **18**, 2065–2071.
8. Absi, J. and Glandus, J. C., Improved method for severe thermal shocks testing of ceramics by water-quenching. *J. Eur. Ceram. Soc.*, 2004, **24**, 2835–2838.
9. Boccaccini, D. N. and Leonelli, C., Thermal shock behaviour of mullite-cordierite refractory materials. *Adv. Appl. Ceram.*, 2007, **106**(3), 142–148.
10. Sebbani, M. J. E. and Allaire, C., Influence of firing temperature on correlation between thermal shock and mechanical impact resistance of refractory castables. *Br. Ceram. Trans.*, 2000, **99**(5), 215–218.
11. Lee, J. K., Lee, J. H. and Lee, S. P., Nondestructive evaluation of damage behavior of ceramic under thermal shock cycle. *Key Eng. Mater.*, 2004, **270–273**, 497–502.
12. Das, A. C., Mukherjee, S., Chaudhury, K., Niyogi, S. K. and Phani, K. K., Crack growth in castable refractory due to thermal shock fatigue: an acousto-ultrasonic study. *Trans. Indian Ceram. Soc.*, 1993, **52**(4), 139–145.
13. Chung, H. W., Ultrasonic testing of concrete after exposure to high temperatures. *NDT Int.*, 1985, **18**(5), 275–278.
14. Kamiya, N., Thermal proof test of ceramics. In *Thermal Shock and Thermal Fatigue Behaviour of Advanced Ceramics*, ed. G. A. Schneider and G. Petzow. Kluwer Academic Publishers, 1993, pp. 473–482.
15. Bao, Y. W., Wang, X. H., Zhang, H. B. and Zhou, Y. C., Thermal shock behavior of Ti_3AlC_2 from between 200 °C and 1300 °C. *J. Eur. Ceram. Soc.*, 2005, **25**, 3367–3374.

16. Aksel, C. and Riley, F. L., Young's modulus measurements of magnesia-spinel composites using load-deflection curves, sonic modulus, strain gauges and Rayleigh waves. *J. Am. Ceram. Soc.*, 2003, **23**, 3089–3096.
17. Aksel, C. and Warren, P. D., Thermal shock parameters R, R′′′, R′′′′ of magnesia-spinel composites. *J. Eur. Ceram. Soc.*, 2003, **23**, 301–308.
18. Soboyejo, W. O. and Mercer, C., Investigation of thermal shock in a high-temperature refractory ceramic: a fracture mechanics approach. *J. Am. Ceram. Soc.*, 2001, **84**(6), 1309–1314.
19. Uzaki, N., Ishii, H., Aratani, K., Kawakami, T. and Sakai, T., Development of magnesite-chrome refractories with high thermal shock resistance. *Interceram*, 1991, **5**, 279–283.
20. Sen, S., Chowdhury, A., Roy, S. K. C. and Ghosh, K. S., Comparative behaviour of fracture and thermal shock behaviour of conventional, low cement and ultra low cement castables. In *Proceedings of Unitecr 97*, 1997, pp. 53–62.
21. Glandus, J. C. and Hugot, F., Thermo-mechanical behavior of structural ceramics submitted to mild thermal shocks. In *Proceedings of Euroceramics V*, 1997, pp. 619–622.
22. Mignard, F., Olagnon, C. and Fantozzi, G., Acoustic emission monitoring of damage evaluation in ceramics submitted to thermal shock. *J. Eur. Ceram. Soc.*, 1995, **15**, 651–653.
23. Aksel, C., Mechanical properties and thermal shock behaviour of alumina–mullite–zirconia and alumina-mullite refractory materials by slip casting. *Ceram. Int.*, 2003, **29**(3), 311–316.
24. Hamidouche, M., Bouaouadja, N., Olagnon, C. and Fantozzi, G., Thermal shock behaviour of mullite ceramic. *Ceram. Int.*, 2003, **29**(6), 599–609.
25. Schneibel, J. H., Sabol, S. M., Morrison, J., Ludeman, E. and Carmichael, C. A., Cyclic thermal shock resistance of several advanced ceramics and ceramic composites. *J. Am. Ceram. Soc.*, 1998, **81**(7), 1888–1892.
26. Panda, P. K., Kannah, T. S., Dubois, J., Olagnon, C. and Fantozzi, G., Thermal shock and thermal fatigue study of ceramic materials on a newly developed ascending thermal shock test equipment. *Sci. Technol. Adv. Mater.*, 2002, **3**, 327–334.
27. Soady, J. S. and Plint, S., A quantitative thermal shock approach to the development of magnesia-spinel refractories for the cement kiln. In *Proceedings of Unitecr 1991*. Aachen, Germany, 1991, pp. 443–449.
28. Panda, P. K., Kannan, T. S., Dubois, J., Olagnon, C. and Fantozzi, G., Thermal shock and thermal fatigue study of alumina. *J. Eur. Ceram. Soc.*, 2002, **22**, 2187–2196.
29. Coppack, T. J., A method for thermal cycling refractories and an appraisal of its effect by a non-destructive technique. *J. Br. Ceram. Soc.*, 1981, **80**(2), 43–46.
30. Meyer-Rau, S. and Telle, R., Testing strategies for corrosive interactions of ceramics with semi-solid and molten metal alloys. *J. Eur. Ceram. Soc.*, 2005, **25**, 1049–1055.
31. Radenthein, M. O., Fully automated thermal shock test method for testing fired refractory brick. *Radex-Rundschau*, 1990, **2–3**, 268–274.
32. Dienst, W., Scholtz, H. and Zimmermann, H., Thermal shock resistance of ceramic materials in melt immerion test. *J. Eur. Ceram. Soc.*, 1989, **5**(6), 365–370.
33. Morita, N., Generation and propagation behavior of laser induced thermal cracks. *J. Ceram. Soc. Jpn.*, 1993, **101**(5), 522–527.
34. Akiyama, S. and Amada, S., A new method to evaluate the thermal shock resistance of ceramics by laser pulse irradiation. *Fusion Technol.*, 1992, **23**, 426–434.
35. Benz, A., Nickel, H., Naoumidis, A., Menzel, S., Wetzig, K. and Rossek, U., Thermal shock behaviour of various first-wall materials under simulation load test by laser beam irradiation. *J. Nucl. Mater.*, 1994, **212–215**, 1318–1322.
36. Mizutani, Y., Nishikawa, T., Fukui, T. and Takatsu, M., Thermal shock fracture of ceramic disc under rapid heating. *J. Ceram. Soc. Jpn., Int. Ed.*, 1995, **103**(5), 525–528.
37. Leatherland, J. L. and Rawlings, R. D., Thermal shock testing of alumina graphite refractories. In *Proceedings of Steelmaking Conference*, 1996, pp. 409–418.
38. Bell, D. A., Thermal shock of magnesia-graphite refractories. In *Proceedings of Unitecr 1991*. Aachen, Germany, 1991, pp. 342–344.
39. Latella, B. A. and Tainshun, L., The initiation and propagation of thermal shock cracks in graphite. *Carbon*, 2006, **44**(14), 3043–3048.
40. Boccaccini, D. N., Romagnoli, M., Veronesi, P., Cannio, M., Leonelli, C. and Pellacani, G. C., Quality control and thermal shock damage characterization of high-temperature ceramics by ultrasonic pulse velocity testing. *Int. J. Appl. Ceram. Technol.*, 2007, **4**(3), 260–268.
41. Boccaccini, D. N., Romagnoli, M., Kamseu, E., Veronesi, P., Leonelli, C. and Pellacani, G. C., Determination of the thermal shock resistance in refractory materials by ultrasonic pulse velocity measurement. *J. Eur. Ceram. Soc.*, 2007, **27**, 1859–1863.
42. Quintela, M. A., Melo, T. M. F., Lage, I. J., Rodrigues, J. A. and Pandolfelli, V. C., Thermal shock resistance of carbon-containing refractories, 2003. *Interceram, Refract. Manual*, 2003.
43. Geck, H. G., Langhammer, H. J. and Chakraborty, A., Kammerofen zur betriebsnahen Prüfung der Temperaturwechselbeständigkeit feuerfester Steine. *Stahl und Eisen*, 1973, **93**(21), 967–976.
44. Yamuna, A., Honda, S., Sumita, K., Yanagihara, M., Hashimoto, S. and Awaij, H., Synthesis, sintering and thermal shock resistance estimation of porous cordierite by IR heating. *Microporous Mesoporous Mater.*, 2005, **85**(1/2), 169–175.
45. Wei, G. C., Hot gas method and apparatus for thermal shock testing. In *Thermal Shock and Thermal Fatigue Behaviour of Advanced Ceramics*, ed. G. A. Schneider and G. Petzow. Kluwer Academic Publishers, 1993, pp. 483–494.
46. Konsztowicz, K. J., Acoustic emission amplitude analysis in crack growth studies during thermal shock of ceramics. In *Thermal Shock and Thermal Fatigue Behaviour of Advanced Ceramics*, ed. G. A. Schneider and G. Petzow. Kluwer Academic Publishers, 1993, pp. 429–441.
47. Tuchozka-Szmeja, B. and Wala, T. B., Thermal shock acoustic emission and microstructure of refractories. I. High alumina refractories (60–90% Al_2O_3). *Ceram. Int.*, 1994, **20**(6), 359–366.
48. Davis, W. R. and Brough, R., Ultrasonic techniques in ceramic research and testing. *Ultrasonics*, 1972(May), 118–126.
49. Posarac, M., Dimitrijevic, M., Volkov-Husovic, T., Devecerski, A. and Matovic, B., Determination of thermal shock resistance of silicon carbide/cordierite composite material using nondestructive test methods. *J. Eur. Ceram. Soc.*, 2008, **6**, 1275–1278.
50. Landis, E. N., Nagy, E. N., Keane, D. T. and Nagy, G., Technique to measure 3D work-of-fracture of concrete in compression. *J. Eng. Mech.*, 1999(June), 599–605.
51. Daigle, M., Fratta, D. and Wang, L. B., Ultrasonic and X-ray tomographic imaging of highly contrasting inclusions in concrete specimens. In *Proceedings of GeoFrontier 2005 Conference*, 2005.
52. Landis, E. N., Towards a physical damage variable for a heterogeneous quasi-brittle material. In *Proceedings of 11th International Conference on Fracture*, 2005, p. 1150.
53. Damhof, F., Brekelmans, W. A. M. and Geers, M. G. D., Non-local modeling of thermal shock damage in refractory materials. *Eng. Frac. Mech.*, 2008, **75**(16), 4706–4720.
54. Chaboche, J. L., Continuum damage mechanics. Part I—General concepts. *J. Appl. Mech.*, 1988, **55**, 59–64.
55. Nentech, W., Meftah, F. and Reynouard, J. F., An elasto-plastic damage model for plain concrete subjected to high temperatures. *Eng. Struct.*, 2002, **24**, 597–611.
56. Luccioni, B. M., Figueroa, M. I. and Danesi, R. F., Thermo-mechanic model for concrete exposed to elevated temperatures. *Eng. Struct.*, 2003, **25**, 729–742.
57. Gawin, D., Majorana, C. E. and Schrefler, B. A., Numerical analysis of hygro-thermal behaviour and damage of concrete at high temperature. *Mech. Coh. Frict. Mater.*, 1999, **4**, 37–44.
58. Hasselman, D. P. H., Thermal stress resistance parameters for brittle refractory ceramics: a compendium. *Am. Ceram. Soc. Bull.*, 1970, **49**(12), 1033–1037.
59. Carslaw, H. S. and Jaeger, J. C., *Conduction of Heat in Solids*. Oxford University Press, 1959, pp. 60–61.

60. Andreev, K. and Harmuth, H., Application of finite element modeling to the thermo-mechanical behaviour of refractories. In *Finite Elements in Civil Engineering Applications*, ed. Hendriks and Rots, 2002, pp. 61–66.
61. Andreev, K. and Harmuth, H., FEM simulation of the thermo-mechanical behaviour and failure of refractories—a case study. *J. Mater. Process.*, 2003, **143–144**, 72–77.
62. Loeb, A. L., Thermal conductivity: VIII, a theory of thermal conductivity of porous materials. *J. Am. Ceram. Soc.*, 1954, **37**(2), 96–99.
63. Aly, F. and Semler, C. E., Prediction of refractory strength using non-destructive sonic measurements. *Am. Ceram. Soc. Bull.*, 1985, **64**(12), 1555–1558.